JACS
JOURNAL OF THE AMERICAN CHEMICAL SOCIETY

ARTICLE

pubs.acs.org/JACS

Polymorphism in Self-Assembled AB_6 Binary Nanocrystal Superlattices

Xingchen Ye,[†,‡] Jun Chen,[§,‡] and Christopher B. Murray*[,†,§]

[†]Department of Chemistry and [§]Department of Materials Science and Engineering, University of Pennsylvania, Philadelphia, Pennsylvania 19104, United States

Supporting Information

ABSTRACT: We report the formation and systematic structural characterization of a new AB_6 polymorph with the body-centered cubic (bcc) symmetry in binary nanocrystal superlattices (BNSLs). The bcc-AB_6 phase, lacking any atomic analogue, is isomorphic to certain alkali-metal intercalation compounds of fullerene C_{60} (e.g., K_6C_{60}). On the basis of the space-filling principle, we further tailor the relative phase stability of the two AB_6 polymorphs—CaB_6 and bcc-AB_6—from coexistence to phase-pure bcc-AB_6, highlighting the entropic effect as the main driving-force of the self-organization of BNSLs. We also discuss the implication of surface topology studies and the observation of twinning and preferential orientation in bcc-AB_6 on the growth mechanism of BNSLs. Furthermore, the connection between the bcc-AB_6 phase and the (3^2.4.3.4) Archimedean tiling shows the promise of further exploration on the structural diversity (both periodic and aperiodic) in this emerging class of metamaterials. The identification and the ability to tune the relative phase stability of polymorphic structures provide a unique opportunity to engineer the interparticle coupling through controlled clustering and/or interconnectivity of sublattice in BNSLs with identical stoichiometry.

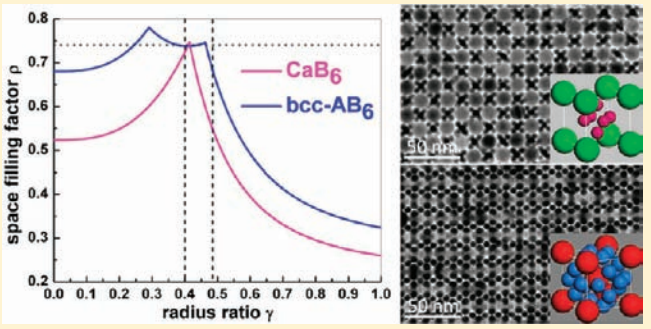

1. INTRODUCTION

Controlled synthesis and organization of molecules, supramolecular complexes, and inorganic nanomaterials into functional superstructures or architectures have been the focus of many materials research efforts.[1−8] Ordered arrays of colloidal nanocrystals (NCs) not only provide opportunities to study self-assembly processes but also offer a low-cost bottom-up approach for integration of nanoscale building blocks into functional devices, including field-effect transistors,[9] thermoelectric converters,[10] light-emitting diodes,[11,12] photodetectors,[13] solar cells,[14] plasmonic waveguides[15] and sensors,[16,17] magnetic recording media.[18] In particular, the modular assembly of two different NCs into binary nanocrystal superlattices (BNSLs) has recently attracted fast-growing research interests, as it provides a versatile means to capture the beauty as well as structural diversity at the nanoscale and more importantly, to access a diverse array of metamaterials with programmable physical properties.[19−24]

From a different perspective, NCs can often be regarded as "artificial atoms" and NC superlattices can serve as a convenient platform to help understand a variety of phenomena and dynamic processes during crystal formation in atomic solids that are usually very hard to visualize in real space.[25] Polymorphism, the ability of a material to exist in more than one form in the solid state, has profound implications for advances of materials science and technology. Perhaps the most amazing demonstration is the polymorphism of carbon. Graphite and diamond are traditional polymorphs, but the discoveries of others such as C_{60},[26] carbon nanotubes,[27] and the most recent one—graphene[28]—have stimulated enormous research activities on the chemistry, physics, and technological applications of these materials and their derivatives. It is notable that alkali-metal fullerides using C_{60} building blocks show dramatic structure−property differences depending on the polymorph: face-centered-cubic K_3C_{60} is superconducting,[29] while no superconductivity is observed in body-centered cubic (bcc) K_3C_{60}.[30]

In this work, we report an experimental study of polymorphism in AB_6 BNSLs self-assembled from monodisperse Au and Fe_3O_4 NCs. We identify a new AB_6 polymorph exhibiting bcc lattice symmetry, which complements the known simple cubic CaB_6 phase. The size ratio between small and large NCs is employed to adjust the relative phase stability between the two AB_6 polymorphs, resulting in the reproducible formation of phase-pure bcc-AB_6 BNSLs.

2. EXPERIMENTAL SECTION

2.1. Synthesis and Characterization of Nanocrystals. All syntheses were performed using standard Schlenk techniques. The

Received: October 6, 2010
Published: February 3, 2011

Fe_3O_4 NCs were synthesized using the method developed by Hyeon et al.[31] The Au NCs were synthesized on the basis of the method developed by Yin et al.[32] for Ag NCs and a digestive ripening route developed by Klabunde et al.[33] for Au NCs. Briefly, 0.08 g of $AuCl_3$ (99.99%, Aldrich) was dissolved in a mixture of 3 mL of oleylamine (70%, Aldrich) and 6 mL of *o*-dichlorobenzene (99%, Acros Organics). The solution was then injected into a boiling mixture (~181 °C) of 0.4 g of 1,2-hexadecanediol (90%, Aldrich) and 12 mL of *o*-dichlorobenzene under nitrogen flow and vigorous magnetic stirring. The reaction mixture was subsequently maintained at 165 °C for 90 s (for 4.6 nm Au NCs, relative standard deviation RSD < 6%) or 3 min (for 5.8 nm Au NCs, RSD < 5%) before it was cooled to room temperature using a water bath. After being isolated by adding ethanol and centrifugation, the Au NCs were then redispersed in 20 mL of toluene in the presence of 2 mL of 1-dodecanthiol (98%, Aldrich), and the mixture was refluxed for 15 min under nitrogen flow. Precipitation with ethanol allows the removal of excess 1-dodecanethiol and isolation of NCs. Finally, the Fe_3O_4 and Au NCs were dissolved in trichloroethylene (TCE, Aldrich, 99.5%) with a NC concentration of ~1.5 and ~0.5 mg/mL, respectively. Particle number concentrations of NC solutions were estimated from thermal gravimetric analysis (TGA). Electrophoretic mobility measurements were performed on a Delsa Nano C system (Beckman Coulter).

2.2. Preparation of Binary Nanocrystal Superlattices. A TEM grid (300 mesh, Electron Microscopy Sciences) was placed at the bottom of a glass vial containing 10 μL of TCE solution of Fe_3O_4 NCs, 15−30 μL of TCE solution of Au NCs, and 100 μL of TCE. The tilted vial (~45° tilt angle) was left inside a vacuum oven under reduced pressure (~30 kPa) at 50 °C. The grid was taken out after 12 h for further structural analysis.

2.3. Structural Characterization of Binary Nanocrystal Superlattices. Transmission electron microscopy (TEM) images and electron diffraction patterns were taken on a JEM1400 transmission electron microscope operating at 120 kV. Tilting of the BNSL structures was performed using a model 2040 dual-axis TEM tomography holder (Fischione Instruments). Three-dimensional crystal structure models were built using Materials Studio 4.4 (Accelrys Software) and were compared with TEM images. Different projections were obtained by direct tilting of the built crystal structures. Electron diffraction simulation was performed using EMS software (Pierre Stadelmann). Scanning electron microscopy (SEM) was carried out on a JEOL 7500F high-resolution SEM. We also performed the two-dimensional Fourier transformation of the real-space TEM images to ensure consistency with the experimental small-angle electron diffraction patterns.

3. RESULTS AND DISCUSSION

3.1. Self-Assembly and Systematic Structural Characterization of CaB_6 and bcc-AB_6 BNSLs. The three-dimensional (3D) structural models of CaB_6 and bcc-AB_6 are shown in parts a and c of Figure 1, respectively. The CaB_6 unit cell consists of a simple cubic lattice of large spheres with an octahedral cluster composed of six small spheres inside. On the other hand, the bcc-AB_6 unit cell consists of a body-centered cubic lattice formed by the large spheres, with the four small spheres forming a square on each of the six faces of the cube. Each large sphere is thus surrounded by 24 small spheres, and all small spheres are equivalent, sitting in the interstitial sites of distorted tetrahedral symmetry created by four large spheres. Therefore, the two AB_6 polymorphs differ in the arrangement of both large and small spheres as well as the lattice symmetry. The bcc-AB_6 structure was first discovered in certain alkali-metal intercalation compounds of fullerene C_{60} (e.g., K_6C_{60}, Cs_6C_{60} etc.).[30] Later on, it

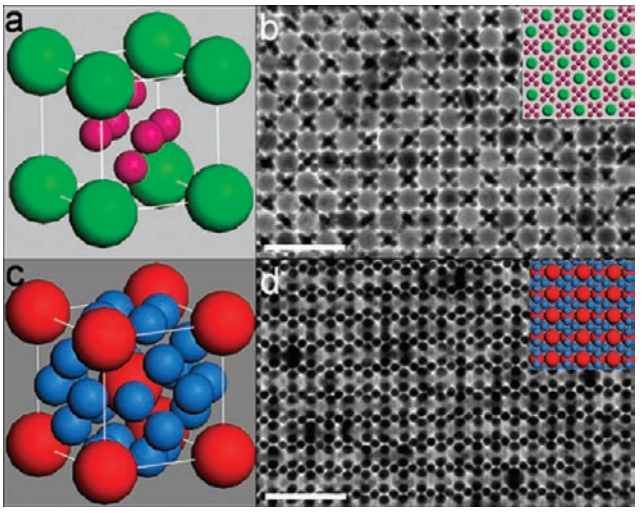

Figure 1. Structural models and TEM images of AB_6 BNSLs self-assembled from 4.6 nm Au and 14.0 nm Fe_3O_4 NCs. Unit cells of (a) CaB_6 and (c) bcc-AB_6 structures. (b) TEM image and structural model (inset) of the [001] projection of CaB_6 BNSLs. (d) TEM image and structural model (inset) of the [110] projection of bcc-AB_6 BNSLs. The scale bars represent 50 nm.

was observed as a stable phase of binary mixtures of hard spheres at size ratio ~0.40[34] and also theoretically predicted and identified in colloidal crystals composed of micrometer-sized oppositely charged particles.[35] Parts b and d of Figure 1 show the TEM images of the commonly observed projections of BNSLs isostructural with CaB_6 and bcc-AB_6 phases, respectively. Both structures are self-assembled from 4.6 nm Au and 14.0 nm Fe_3O_4 NCs (RSD < 4%) under slow evaporation of a combined TCE solution (see section 2.2). Importantly, they coexist in a single sample under certain preparation conditions (e.g., when solutions with ~1:8 Fe_3O_4-to-Au NC number ratio are used). The TEM image shown in Figure 1b matches the [001] projection of the CaB_6 structure in which the $(Au)_6$ octahedral clusters are separated by the simple cubic packed Fe_3O_4 NCs. Moreover, the characteristic alternating chains of Au and Fe_3O_4 NCs shown in Figure 1d are consistent with the [110] projection of the bcc-AB_6 structure. This suggests a previously unidentified bcc polymorph of AB_6 BNSL.

It has been shown that, in BNSLs, domains corresponding to either different crystal structures or different projections of the same crystal structures can be observed in a single sample.[24,36−44] The visual comparison of TEM images with the projections of modeled crystal structures could lead to misinterpretation of the 3D arrangement of NCs in BNSLs. Therefore, to unambiguously assign the structure of BNSLs, we need to obtain local and global structural information from BNSL domains.[41,42,45] Here we apply the general structural characterization framework to the study of polymorphism in AB_6 BNSLs.[41] The "toolset" includes a combination of techniques: stereographic projection is used as a crystallographic tool to design series tilt path. TEM images and small-angle electron diffraction (SAED) patterns acquired during series tilting provide direct real-space and reciprocal-space information of the BNSL structures. Modeling of crystallographic projections and simulation of electron diffraction patterns help interpret and confirm the experimental data. In this study, we also use SEM to investigate the surface topology of the bcc-AB_6 BNSLs, which provides complementary and particularly

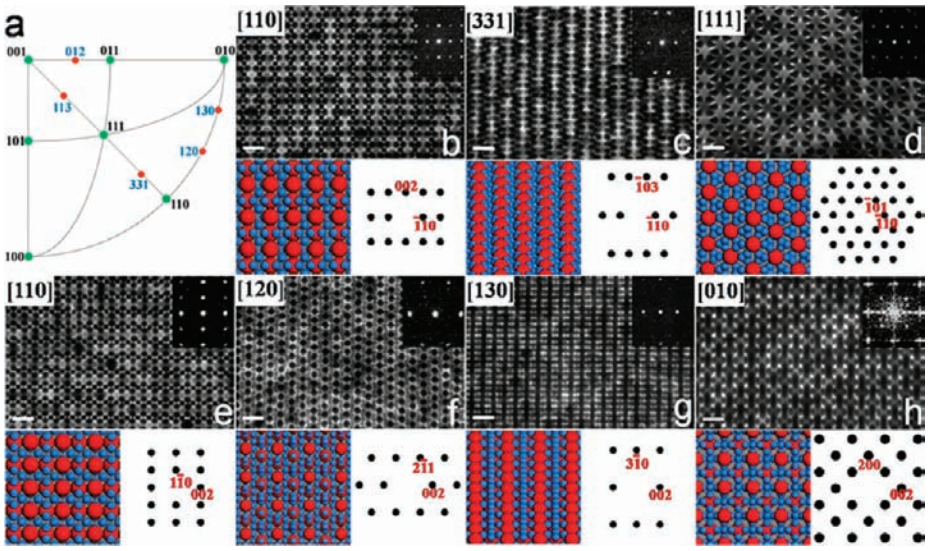

Figure 2. Series tilting of bcc-AB_6 BNSLs self-assembled from 4.6 nm Au and 14.0 nm Fe_3O_4 NCs. (a) Stereographic projection of the cubic crystal system. The projection plane is normal to the [001] direction. Tilt series 1 (b−d) starts from the [110] zone axis and tilts around the [$\bar{1}$10] direction. Tilting sequence: [110]→[331]→[111]. After 90° in-plane rotation of b, tilt series 2 (e−h) starts from the [110] zone axis and tilts around the [001] direction. Tilting sequence: [110]→[120]→[130]→[010]. Below each TEM image (inset of each is the corresponding small-angle ED pattern) are the corresponding structural model (left) and simulated ED pattern (right) except that the upper-right inset of part h is the corresponding fast Fourier transform pattern. All scale bars represent 20 nm.

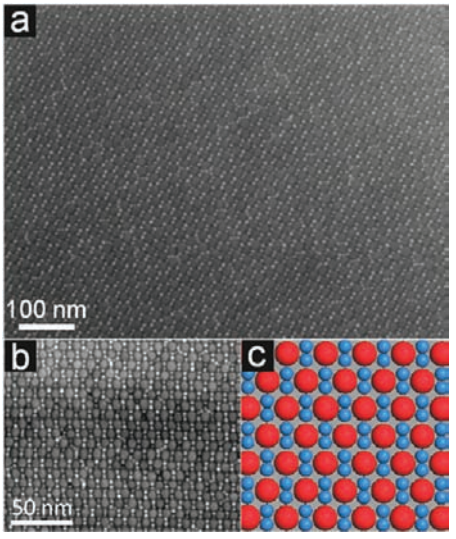

Figure 3. (a, b) SEM images of the bcc-AB_6 BNSLs self-assembled from 4.6 nm Au and 14.0 nm Fe_3O_4 NCs. (c) Structural model of the (110) plane of CaB_6 BNSLs.

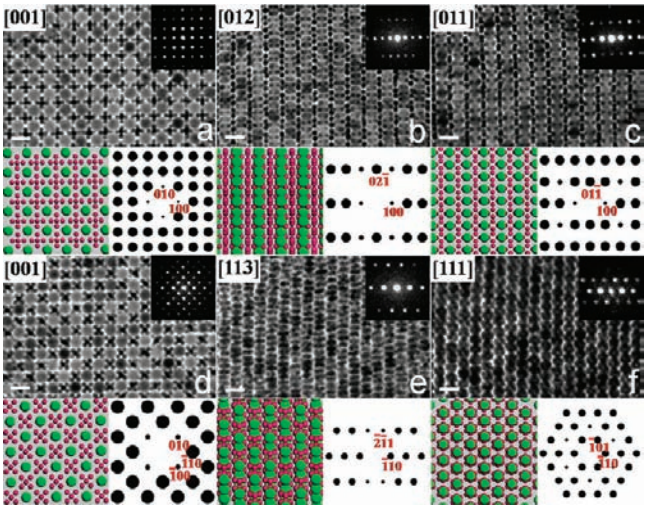

Figure 4. Series tilting of CaB_6 BNSLs self-assembled from 4.6 nm Au and 14.0 nm Fe_3O_4 NCs. Tilt series 1 (a−c) starts from the [001] zone axis and tilts around the [100] direction. Tilting sequence: [001]→[012]→[011]. After 45° in-plane rotation of a, tilt series 2 (d−f) starts from the [001] zone axis and tilts around the [$\bar{1}$10] direction. Tilting sequence: [001]→[113]→[111]. Below each TEM image (inset of each is the corresponding small-angle ED pattern) are the corresponding structural model (left) and simulated ED pattern (right). All scale bars represent 20 nm.

useful structural information for the identification of the bcc-AB_6 polymorph.[40]

According to the stereographic projection of the cubic lattice (Figure 2a), we design two series tilting paths connecting low-index projections such as [001], [011], and [111] for the bcc-AB_6 BNSLs. The TEM images and SAED patterns of projections obtained during series tiltings are presented in Figure 2. The correspondence between the TEM images of six different crystallographic projections and the models and the consistency between real and simulated SAED patterns confirm the bcc-AB_6 structure. Furthermore, the SEM images acquired from bcc-AB_6 BNSLs (Figures 3a,b and S4, Supporting Information) display a particle packing motif different from what is observed in the TEM images. The arrangement of surface NCs matches the model of the (110) plane (Figure 3c). These electron microscopy surveys yield a unique structural assignment of the BNSLs shown in Figure 1d as bcc-AB_6.

To further compare the structural difference among various projections of the two AB_6 polymorphs, we perform series tilting experiments on CaB_6 BNSLs (Figure 4). Although formation of the CaB_6 structure has been reported in PbSe−Pd and

dx.doi.org/10.1021/ja108708v |J. Am. Chem. Soc. 2011, 133, 2613–2620

Fe_2O_3−Au BNSLs,[22,23] to the best of our knowledge, no TEM tilting study has been carried out. As shown in Figure 4, TEM images of other projections of CaB_6 BNSLs including [012], [011], [113], and [111] projections are seen after series tilting from the [001] projection. Again all the projections are in accordance with the structural models, further confirming the 3D packing of NCs in the CaB_6 structure.

3.2. Tuning of Polymorphism in AB_6 BNSLs Based upon Packing Density Consideration. To date, various interparticle interactions have been taken into account to understand the formation mechanism and structural diversity of BNSLs, including free volume entropy (space-filling principle),[38,39,41,42,44,46] electrostatic couloumb interactions,[21,22,38,47] dipole−dipole interactions,[38,46] van der Waals forces between the NCs[38,42] and hydrophobic interactions between the ligands.[38,39] Among these, the free volume entropy and the electrostatic interactions have been shown to be able to contribute significantly to the overall energy landscape during self-assembly of NCs and thus affect the structure of BNSLs.[21,22,46] To explore the contribution of electrostatic interaction to the relative phase stability of the two AB_6 polymorphs, we performed electrophoretic mobility measurements on Au and Fe_3O_4 NCs dispersed in TCE solvent. The Fe_3O_4 and Au NCs employed in this study are capped with oleic acid and 1-dodecanethiol molecules, respectively. The results, as shown in Figure S5 (Supporting Information), demonstrate that both NCs are nearly electrostatically neutral. Therefore, we believe that the formation of both CaB_6 and bcc-AB_6 BNSLs in this study is mainly entropy-driven (see discussion below).

The total entropy of a hard sphere system consists of two parts: the configurational entropy and the free volume entropy.[48,49] The former relates to the degree of spatial ordering and the latter is associated with the free space available for individual particle's local movements. Entropy-driven crystallization is achieved when the increase in free volume entropy is greater than the decrease in configurational entropy. This simple entropic origin is the driving force for superlattice formation in hard sphere systems.[48,50] Superlattice structures with a higher packing density should have a larger free volume per particle, thus offering a larger contribution to the entropy and hence a lower free energy. Therefore, the ensemble of hard spheres should adopt an ordered lattice structure that maximizes the packing density.[51−53]

As far back as the 1960s, Parthé used the packing arguments to explain the phase stability of some binary intermetallic alloys.[54] Later on in the 1980s, Sanders and Murray reported observations of long-range ordered close-packed structures in natural opals composed of silica spheres of two different sizes.[55,56] These stimulated theoretical efforts where the packing density of the observed structures (namely AlB_2 and $NaZn_{13}$) was calculated in more detail.[57] Since most sterically stabilized (uncharged) colloidal particles can be approximated as hard spheres,[58,59] we extend the geometrical analysis of Murray and Sanders to the bcc-AB_6 phase. This provides a good estimate of the entropic contribution to the phase stability of the bcc-AB_6 structure. The space-filling curves for the bcc-AB_6 and CaB_6 structures (ρ versus γ, where ρ = space-filling factor and γ = radius ratio between small and large spheres) are shown in Figure 5a.

In the case of the bcc-AB_6 structure, the first branch of the space filling curve corresponds to the low γ region where there are only A−A contacts. Here B spheres are small enough and

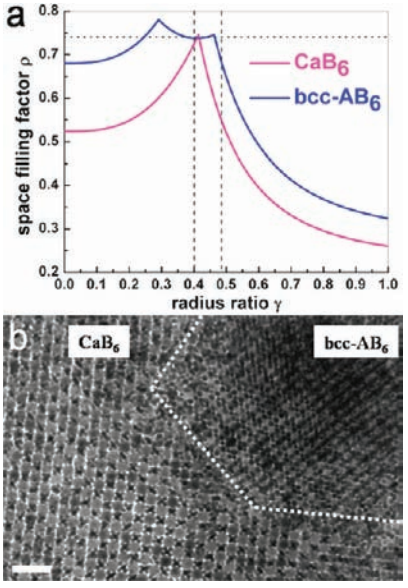

Figure 5. (a) Space-filling curves of CaB_6 and bcc-AB_6 structures. The horizontal dashed line represents the packing density $\rho = 0.7405$ of the single-component close-packed structures. The vertical dashed lines denote the radius ratio γ studied in this work. (b) TEM image showing the coexistence of CaB_6 and bcc-AB_6 structures in BNSLs self-assembled from 4.6 nm Au and 14.0 nm Fe_3O_4 NCs. The scale bar represents 50 nm.

the lattice parameter is determined only by the radius of A spheres. The packing density of this region is given by

$$\rho = \frac{\sqrt{3}\pi}{8}(1 + 6\gamma^3)$$

The formula is valid until contacts between small and large spheres occur at $\gamma \approx 0.291$. Then the second branch of the space-filling curve corresponds to a situation where both A−A and A−B contacts occur, and the lattice parameter is determined by the size ratio γ. The packing density of this region is given by

$$\rho = \frac{5\sqrt{5}\pi}{24}(1 + 6\gamma^3)(1+\gamma)^3$$

The upper limit of the second branch is reached when B−B contacts occur at $\gamma \approx 0.462$. The third branch corresponds to the situation where there are only B−B contacts, and the lattice parameter is solely determined by the radius of B spheres. The packing density of this region is given by

$$\rho = \frac{\sqrt{2}\pi}{96}(6+\gamma^{-3})$$

The space-filling curve of the bcc-AB_6 structure features a high packing density zone with $\rho \geq 0.7405$ (the packing density of single-component close-packed structures) in the region of $0.245 < \gamma < 0.465$. In this study, the effective size of NCs d_{eff} can be estimated as $d_{eff} = d_{core} + 2d_{shell}$, where d_{core} is the diameter of the inorganic core measured from TEM images and d_{shell} is the effective thickness of the ligand shell.[38] Therefore, d_{eff} of the 4.6 nm Au NCs is estimated to be ~6.3 nm and d_{eff} of the 14.0 nm Fe_3O_4 NCs is ~15.7 nm, giving rise to a size ratio γ of ~0.40, which falls into the "stable zone" of the bcc-AB_6 structure. The same size ratio gives a packing fraction of ~0.738

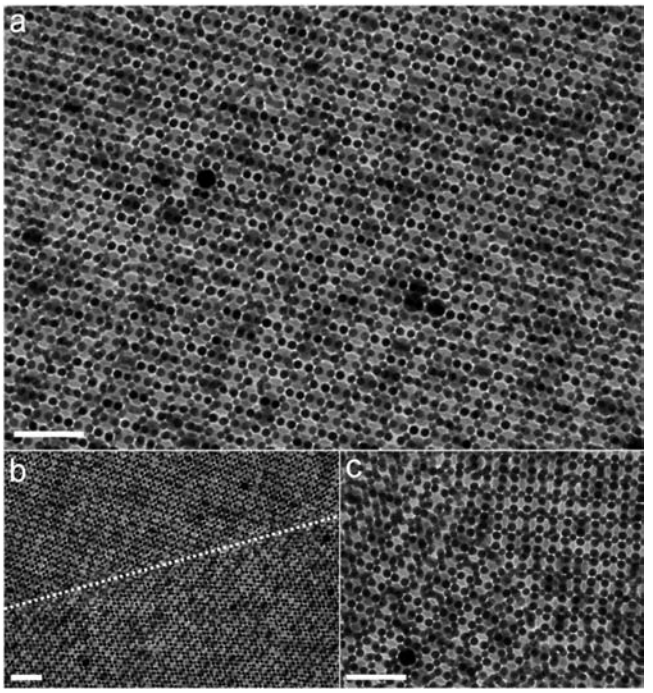

Figure 6. (a) TEM image of a [110]-oriented domain of bcc-AB_6 BNSLs self-assembled from 5.8 nm Au and 14.0 nm Fe_3O_4 NCs. (b) Low and (c) high magnification TEM images of twin boundaries (highlighted with dash line) in bcc-AB_6 BNSLs self-assembled from 5.8 nm Au and 14.0 nm Fe_3O_4 NCs. All scale bars represent 50 nm.

for the CaB_6 structure. Therefore, we believe that the reason for the polymorphism in AB_6 BNSLs is mainly due to the high packing density of both structures at this size ratio ($\gamma \sim 0.40$), i.e., entropy-driven self-assembly process (Figures 5a,b and S6, Supporting Information). In addition, since the two polymorphs are different in their arrangement of both large and small NCs, the transformation between the two structures may involve a large change in free energy and/or a large activation barrier and thus is very unlikely. In fact, samples are found to retain the same structure after 2 years. This further supports that both polymorphs reported here are stable under ambient conditions.

Realizing the coexistence of two polymorphs in the same BNSL sample, we then target the possibility of tuning the relative phase stability between the two structures. The ability to make phase-pure BNSLs is essential to the development of rigorous structure−property relationships for this important class of metamaterials.[24] Size ratio[46] and temperature[42,44] have been invoked as structure-directing factors to affect the stability of one BNSL phase with respect to another. In this case, when the size of Au NCs is increased from 4.6 to 5.8 nm (d_{eff} from 6.3 to 7.5 nm) while the Fe_3O_4 NCs are kept unchanged, long-range ordered bcc-AB_6 BNSLs are formed reproducibly without the coexistence of CaB_6 structure (Figures 6a and S7, Supporting Information). As predicted by the space-filling curves, the increase in the size of Au NCs (~20%) is effective enough to generate phase purity. The size ratio γ between the two components is shifted from ~0.40 to ~0.48, leading to a significant difference between the packing densities of the two polymorphs (~25%).

3.3. Preferential Orientation and Twinning in bcc-AB_6 BNSLs. It has been shown that in BNSL samples, certain

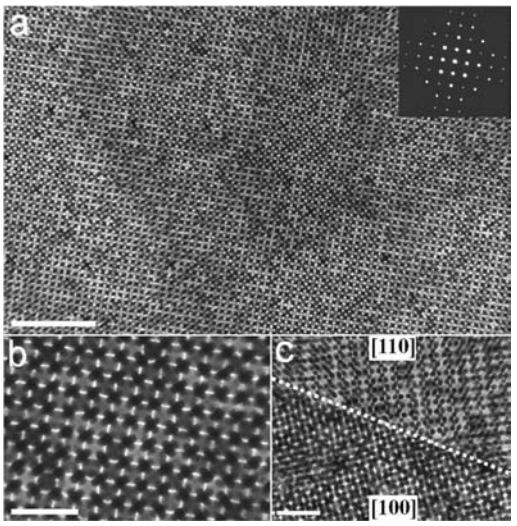

Figure 7. (a) Low and (b) high magnification TEM images of a [100]-oriented domain of bcc-AB_6 BNSLs self-assembled from 5.8 nm Au and 14.0 nm Fe_3O_4 NCs. Inset of part a is the corresponding small-angle ED pattern. (c) TEM image showing the coexistence of [100]- and [110]-oriented domains in bcc-AB_6 BNSLs self-assembled from 5.8 nm Au and 14.0 nm Fe_3O_4 NCs. Scale bars: (a) 200 nm, (b) 50 nm, and (c) 50 nm.

low-index crystallographic projections can be predominate over others, depending on the structure of the BNSL. For example, the [100]- and [110]-oriented domains are statistically more probable than others in ico-AB_{13} BNSLs,[41] while [001] can be the dominant projection in AlB_2-type BNSLs.[40] Chen et al. suggested that coexistence of different projections in BNSL samples might be a result of local fluctuations of NC number ratio and concentration during drying,[46] but a consensus on the dominant factors for preferential orientation has not been reached.

In the case of AB_6 BNSLs self-assembled from 4.6 nm Au and 14.0 nm Fe_3O_4 NCs, we observe exclusively the [100]-oriented domains for CaB_6 BNSLs (Figure S8, Supporting Information) and the [110]-oriented domains for bcc-AB_6 BNSLs (Figure S9, Supporting Information). However, in bcc-AB_6 BNSLs self-assembled from 5.8 nm Au and 14.0 nm Fe_3O_4 NCs, we also observe [100]-oriented domains (Figures 7 and S10, Supporting Information), yet they are much less probable compared to [110]-oriented domains (based upon statistical analysis of ~400 domains from 15 samples). Series tilting experiments starting from [100]-oriented domains in untilted samples further confirm the bcc-AB_6 structure (Figure S11, Supporting Information). The preferential orientation in AB_6 BNSLs might be the result of the lowest energy crystallographic planes in the respective phases, yet we are reluctant to draw any conclusions before in-depth theoretical analysis and further experimental studies are carried out. On the other hand, these well-oriented BNSL facets provide a potential platform for the controlled growth of hetero-structured BNSLs through colloidal epitaxy.[60]

More interestingly, as shown in Figures 6b,c and S7 (Supporting Information), it is commonly seen in the bcc-AB_6 BNSL samples that the lateral extension of the [110]-oriented domains is often disrupted by the mirror reflection of the planes across a sharp interface, i.e., twin boundary. This is in stark contrast with the typical mosaic texture with narrow and often amorphous boundaries separating different oriented domains in other types of BNSLs.[38,41] Rupich et al. recently reported the size-dependent multiple twinning in self-assembled single-component NC

superlattices, demonstrating the potential of using colloidal NCs as model systems for the study of not only periodic ordering but also phenomena such as faceting, defects, and twinning that are present in atomic crystals.[61] As manifested in Figure S12 (Supporting Information), the presence of terraces and twin planes between [110]-oriented domains of the bcc-AB_6 BNSL may imply that the BNSLs grow through a "quasi" layer-by-layer mode, where the addition of a new layer of NCs occurs after substantial lateral growth of the underlying layer.

3.4. Connections of bcc-AB_6 Structure to (3^2.4.3.4) Archimedean Tiling in BNSLs. The recently discovered dodecagonal quasicrystal BNSLs not only are beautiful in their structural complexity but may provide more universal insights into the formation of a broad family of quasicrystalline and aperiodic structures.[23,62−65] It is believed that rather than complex interactions between the NCs, entropy or simple sphere-packing can explain the formation of these complex phases. The aperiodicity generated through the random arrangement of equilateral triangles and squares could be a result of maximizing not only free volume entropy (packing) but also configurational entropy during the self-assembly process.[23] In BNSL samples, the triangles and squares correspond to the regular arrangement of $(Au)_6$ and individual Au NCs separated by Fe_3O_4 NCs, giving rise to the so-called (3^2.4.3.4) and (3^3.4^2) periodic Archimedean tilings with a stoichiometry of AB_4.

Realizing the comparable size ratio γ of the 4.6 nm Au-14.0 nm Fe_3O_4 combination in this work to the reported γ of ∼0.43 for quasicrystalline order in BNSLs, we further exploit the possibility of Archimedean tiling-based aperiodic ordering by adjusting the relative concentration of Au and Fe_3O_4 NCs in the colloidal solution used for BNSL formation. When the Fe_3O_4-to-Au NC number ratio is lowered to ∼1:5, we observe the formation of large-area (3^2.4.3.4) tiling, together with a small fraction of bcc-AB_6 domains in a single sample (Figures 8 and S13, Supporting Information). The sharp spots on the fast-Fourier transform pattern from the (3^2.4.3.4) tiling indicate its 4-fold rotational symmetry (Figure 8a). This suggests that in the absence of other significant interactions, entropy is the dominant driving force for BNSL formation, while fine-tuning of the concentration ratio between the constituents offers an effective means to access several candidate structures predicted by the packing argument.[24,41,66]

3.5. Remarks on the Design Principles and Formation of BNSLs. In the section, we will address several remaining issues, discuss the implications of the observation of polymorphism in AB_6 BNSLs, and make some general remarks on the design of BNSLs.

First, the 2D arrangement of NCs seen in the SEM image of the bcc-AB_6 BNSLs is interesting in its own right: surrounding each Fe_3O_4 NCs are four pairs of smaller Au NCs. This 2D packing motif corresponding to an AB_2 stoichiometry is one of the densest ways to pack spheres in 2D for this particular size ratio (isostructural to the so-called T_1 phase predicted by Likos et al.[67]). This observation might imply that during the formation of bcc-AB_6 BNSLs, NCs first nucleate laterally in 2D followed by growth of a few unit cells in the perpendicular direction. This may also explain the preferential orientation of the AB_6 BNSLs as mentioned above.

Second, we have been employing the space-filling principle to explain/understand the polymorphism in AB_6 BNSLs, but the space-filling factor can only tell us which crystal structures are possible, not which one will form under certain experimental conditions. Introduction or identification of a new phase might also suggest the reduction of the "stability zone" of the existing phases. In this study, we are not able to produce phase-pure CaB_6 BNSLs, no matter how we adjust the number ratio between the NCs for the two size ratios, although the tunability is achieved for the case of the new polymorph—bcc-AB_6.

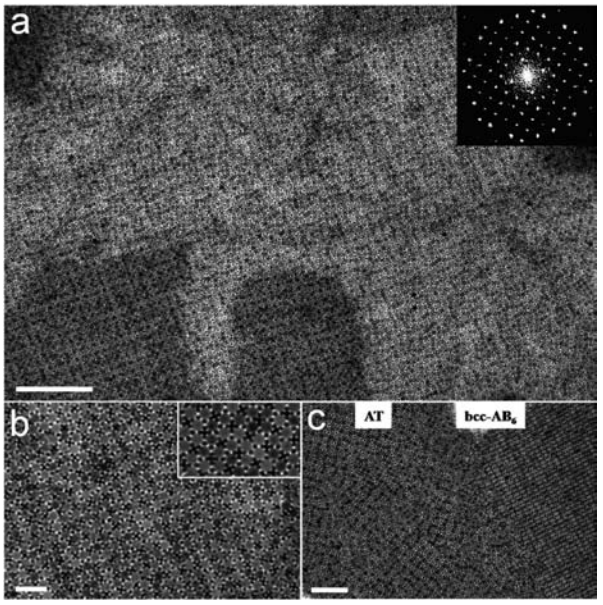

Figure 8. (a, b) TEM images of BNSLs self-assembled from 4.6 nm Au and 14.0 nm Fe_3O_4 NCs exhibiting the packing motif of the periodic (3^2.4.3.4) Archimedean tiling (AT). Inset of part a is the corresponding fast Fourier transform pattern of the superlattices. (c) TEM image showing the coexistence of AT and bcc-AB_6 BNSLs self-assembled from 4.6 nm Au and 14.0 nm Fe_3O_4 NCs. Scale bars: (a) 200 nm, (b) 50 nm, and (c) 100 nm.

According to the space-filling principle, a stable BNSL structure should be the one whose packing density exceeds that of the single-component close-packed structures of large and small spheres (∼0.7405), although experimental results for BNSLs do not always rigorously follow the theoretical prediction. For example, the 5.8 nm Au and 14.0 nm Fe_3O_4 NCs can form bcc-AB_6 BNSLs with a calculated space-filling factor $\rho \sim 0.70$. In fact, rigorous free energy calculations also suggest binary phases with ρ slightly below 0.7405 can still exist, being stabilized by the entropy of mixing and extra configurational entropy.[68] In a real binary NC system, the matter can be further complicated by the interparticle interactions.[21,69−71] However, we still find that theoretical phase stability calculations based upon hard sphere approximation (i.e., space-filling principle) can serve as a qualitative yet useful experimental guide to the BNSL structures expected for a given size ratio and range of the size ratios needed in order to form a particular BNSL phase. Therefore, we provide a library of space-filling curves covering the full range of radius ratios for the majority of BNSL structures that have been reported and predicted (Figure S14, Supporting Information). Several questions still remain: how can one tune the relative phase stability between the NaCl and NiAs structures which have identical space-filling curves and stoichiometry (or the same question regarding the three Lavés phases)? Is there a limit to the complexity of periodic and aperiodic BNSL phases that can be designed?[72] Thanks to the recent development of new deposition methodology for BNSLs, we can now access a variety of

BNSL phases over extended area (cm^2 scale).[24] We anticipate that in the near future many known BNSL phases can become available over that length scale. On the other hand, further development of surface/ligand chemistry of colloidal NC building blocks may help the introduction of higher order or "non-hard-sphere" interparticle interactions into the colloidal NC system in a well-controlled manner, which could enrich the possible BNSL structures to be discovered.[21,73]

4. CONCLUSIONS

We have identified a new AB_6 polymorph—bcc-AB_6—in BNSLs composed of nearly electrostatically neutral Au and Fe_3O_4 NCs through systematic electron microscopy studies. The two AB_6 polymorphs—CaB_6 and bcc-AB_6—differ in their 3D arrangement of both small and large spheres, in their lattice symmetry, and in their space-filling factor. Upon the basis of the space-filling principle, we further demonstrate the possibility of tailoring the relative phase stability between the AB_6 polymorphs by adjusting the size ratio between the two NCs, highlighting the entropic contribution as the main driving force during the self-organization of NCs into BNSLs. In addition, studies of the arrangement of NCs on the BNSLs surface together with the interesting observation of twinning and preferential orientation in bcc-AB_6 BNSLs is indicative of a possible growth mechanism: a close-packed monolayer composed of two types of NCs forms initially followed by growth into 3D BNSLs. BNSLs exhibit unique electronic,[10] plasmonic,[21] or magnetic[24] couplings between the NCs, and the ability to engineer specific polymorphs provides a more powerful route to programmable physical properties.

■ ASSOCIATED CONTENT

Supporting Information. TEM images of Fe_3O_4 and Au NCs, XRD pattern of 4.6 nm Au NCs, electrophoretic mobility measurements of Fe_3O_4 and Au NCs dispersed in TCE, additional TEM and SEM images showing the long-range ordering and twinning in bcc-AB_6 BNSLs and their coexistence with CaB_6 structure and (3^2.4.3.4) Archimedean tiling, tilt series of bcc-AB_6 BNSLs starting from [100]-oriented domains, and a library of space-filling curves and the mathematical expressions for each branch of the curves. This material is available free of charge via the Internet at http://pubs.acs.org.

■ AUTHOR INFORMATION

Corresponding Author

cbmurray@sas.upenn.edu

Author Contributions

‡These authors contributed equally.

■ ACKNOWLEDGMENT

We acknowledge financial support from the Department of Energy Basic Energy Science division through award DE-SC0002158 for synthesis of plasmonic NCs and assembly and characterization of BNSLs (X.Y.) and the Army Research Office (ARO) through MURI award W911NF-08-1-0364 for support of magnetic NC synthesis and assembly and characterization of BNSLs (J.C. and C.B.M.). C.B.M. also thanks the Richard Perry University Professorship for partial support of his supervisor role. We thank Douglas M. Yates and Lolita Rotkina at the Penn Regional Nanotechnology Facility for support in electron microscopy and Benjamin T. Diroll for manuscript proofreading and discussions.

■ REFERENCES

(1) Murray, C. B.; Kagan, C. R.; Bawendi, M. G. *Science* **1995**, *270*, 1335–1338.
(2) Moulton, B.; Zaworotko, M. J. *Chem. Rev.* **2001**, *101*, 1629–1658.
(3) Eddaoudi, M.; Moler, D. B.; Li, H. L.; Chen, B. L.; Reineke, T. M.; O'Keeffe, M.; Yaghi, O. M. *Acc. Chem. Res.* **2001**, *34*, 319–330.
(4) Alivisatos, A. P. *Science* **1996**, *271*, 933–937.
(5) Xia, Y. N.; Yang, P. D.; Sun, Y. G.; Wu, Y. Y.; Mayers, B.; Gates, B.; Yin, Y. D.; Kim, F.; Yan, Y. Q. *Adv. Mater.* **2003**, *15*, 353–389.
(6) Murray, C. B.; Kagan, C. R.; Bawendi, M. G. *Annu. Rev. Mater. Sci.* **2000**, *30*, 545–610.
(7) Pileni, M. P. *Acc. Chem. Res.* **2008**, *41*, 1799–1809.
(8) Nie, Z. H.; Petukhova, A.; Kumacheva, E. *Nat. Nanotechnol.* **2010**, *5*, 15–25.
(9) Talapin, D. V.; Murray, C. B. *Science* **2005**, *310*, 86–89.
(10) Urban, J. J.; Talapin, D. V.; Shevchenko, E. V.; Kagan, C. R.; Murray, C. B. *Nat. Mater.* **2007**, *6*, 115–121.
(11) Colvin, V. L.; Schlamp, M. C.; Alivisatos, A. P. *Nature* **1994**, *370*, 354–357.
(12) Coe, S.; Woo, W. K.; Bawendi, M.; Bulovic, V. *Nature* **2002**, *420*, 800–803.
(13) Konstantatos, G.; Howard, I.; Fischer, A.; Hoogland, S.; Clifford, J.; Klem, E.; Levina, L.; Sargent, E. H. *Nature* **2006**, *442*, 180–183.
(14) Huynh, W. U.; Dittmer, J. J.; Alivisatos, A. P. *Science* **2002**, *295*, 2425–2427.
(15) Maier, S. A.; Kik, P. G.; Atwater, H. A.; Meltzer, S.; Harel, E.; Koel, B. E.; Requicha, A. A. G. *Nat. Mater.* **2003**, *2*, 229–232.
(16) Anker, J. N.; Hall, W. P.; Lyandres, O.; Shah, N. C.; Zhao, J.; Van Duyne, R. P. *Nat. Mater.* **2008**, *7*, 442–453.
(17) Tao, A.; Sinsermsuksakul, P.; Yang, P. *Nat. Nanotechnol.* **2007**, *2*, 435–440.
(18) Sun, S. H.; Murray, C. B.; Weller, D.; Folks, L.; Moser, A. *Science* **2000**, *287*, 1989–1992.
(19) Kiely, C. J.; Fink, J.; Brust, M.; Bethell, D.; Schiffrin, D. J. *Nature* **1998**, *396*, 444–446.
(20) Redl, F. X.; Cho, K. S.; Murray, C. B.; O'Brien, S. *Nature* **2003**, *423*, 968–971.
(21) Kalsin, A. M.; Fialkowski, M.; Paszewski, M.; Smoukov, S. K.; Bishop, K. J. M.; Grzybowski, B. A. *Science* **2006**, *312*, 420–424.
(22) Shevchenko, E. V.; Talapin, D. V.; Kotov, N. A.; O'Brien, S.; Murray, C. B. *Nature* **2006**, *439*, 55–59.
(23) Talapin, D. V.; Shevchenko, E. V.; Bodnarchuk, M. I.; Ye, X. C.; Chen, J.; Murray, C. B. *Nature* **2009**, *461*, 964–967.
(24) Dong, A. G.; Chen, J.; Vora, P. M.; Kikkawa, J. M.; Murray, C. B. *Nature* **2010**, *466*, 474–477.
(25) Wang, Z. L. *Adv. Mater.* **1998**, *10*, 13–30.
(26) Kroto, H. W.; Heath, J. R.; Obrien, S. C.; Curl, R. F.; Smalley, R. E. *Nature* **1985**, *318*, 162–163.
(27) Iijima, S. *Nature* **1991**, *354*, 56–58.
(28) Geim, A. K.; Novoselov, K. S. *Nat. Mater.* **2007**, *6*, 183–191.
(29) Stephens, P. W.; Mihaly, L.; Lee, P. L.; Whetten, R. L.; Huang, S. M.; Kaner, R.; Deiderich, F.; Holczer, K. *Nature* **1991**, *351*, 632–634.
(30) Zhou, O.; Fischer, J. E.; Coustel, N.; Kycia, S.; Zhu, Q.; McGhie, A. R.; Romanow, W. J.; McCauley, J. P.; Smith, A. B.; Cox, D. E. *Nature* **1991**, *351*, 462–464.
(31) Park, J.; An, K. J.; Hwang, Y. S.; Park, J. G.; Noh, H. J.; Kim, J. Y.; Park, J. H.; Hwang, N. M.; Hyeon, T. *Nat. Mater.* **2004**, *3*, 891–895.
(32) Yin, Y. D.; Erdonmez, C.; Aloni, S.; Alivisatos, A. P. *J. Am. Chem. Soc.* **2006**, *128*, 12671–12673.
(33) Stoeva, S.; Klabunde, K. J.; Sorensen, C. M.; Dragieva, I. *J. Am. Chem. Soc.* **2002**, *124*, 2305–2311.

(34) Pusey, P. N. *Faraday Discuss.* **2003**, *123*, 177.
(35) Hynninen, A. P.; Christova, C. G.; van Roij, R.; van Blaaderen, A.; Dijkstra, M. *Phys. Rev. Lett.* **2006**, *96*, 138308.
(36) Saunders, A. E.; Korgel, B. A. *ChemPhysChem* **2005**, *6*, 61–65.
(37) Shevchenko, E. V.; Talapin, D. V.; O'Brien, S.; Murray, C. B. *J. Am. Chem. Soc.* **2005**, *127*, 8741–8747.
(38) Shevchenko, E. V.; Talapin, D. V.; Murray, C. B.; O'Brien, S. *J. Am. Chem. Soc.* **2006**, *128*, 3620–3637.
(39) Chen, Z. Y.; Moore, J.; Radtke, G.; Sirringhaus, H.; O'Brien, S. *J. Am. Chem. Soc.* **2007**, *129*, 15702–15709.
(40) Smith, D. K.; Goodfellow, B.; Smilgies, D.-M.; Korgel, B. A. *J. Am. Chem. Soc.* **2009**, *131*, 3281–3290.
(41) Chen, J.; Ye, X. C.; Murray, C. B. *ACS Nano* **2010**, *4*, 2374–2381.
(42) Bodnarchuk, M. I.; Kovalenko, M. V.; Heiss, W.; Talapin, D. V. *J. Am. Chem. Soc.* **2010**, *132*, 11967–11977.
(43) Overgaag, K.; Evers, W.; de Nijs, B.; Koole, R.; Meeldijk, J.; Vanmaekelbergh, D. *J. Am. Chem. Soc.* **2008**, *130*, 7833–7834.
(44) Evers, W. H.; Nijs, B. D.; Filion, L.; Castillo, S.; Dijkstra, M.; Vanmaekelbergh, D. *Nano Lett.* **2010**, *10*, 4235–4241.
(45) Friedrich, H.; Gommes, C. J.; Overgaag, K.; Meeldijk, J. D.; Evers, W. H.; de Nijs, B.; Boneschanscher, M. P.; de Jongh, P. E.; Verkleij, A. J.; de Jong, K. P.; van Blaaderen, A.; Vanmaekelbergh, D. *Nano Lett.* **2009**, *9*, 2719–2724.
(46) Chen, Z.; O'Brien, S. *ACS Nano* **2008**, *2*, 1219–1229.
(47) Sun, Z. Y.; Luo, Z. P.; Fang, J. Y. *ACS Nano* **2010**, *4*, 1821–1828.
(48) Eldridge, M. D.; Madden, P. A.; Frenkel, D. *Nature* **1993**, *365*, 35–37.
(49) Trizac, E.; Eldridge, M. D.; Madden, P. A. *Mol. Phys.* **1997**, *90*, 675–678.
(50) Bolhuis, P. G.; Frenkel, D.; Mau, S. C.; Huse, D. A. *Nature* **1997**, *388*, 235–236.
(51) Schofield, A. B.; Pusey, P. N.; Radcliffe, P. *Phys. Rev. E* **2005**, *72*, 031407.
(52) Hynninen, A. P.; Filion, L.; Dijkstra, M. *J. Chem. Phys.* **2009**, *131*, 064902.
(53) Frenkel, D. *Nat. Mater.* **2006**, *5*, 85–86.
(54) Parthe, E. *Z. Kristallogr.* **1961**, *115*, 52–79.
(55) Sanders, J. V.; Murray, M. J. *Nature* **1978**, *275*, 201–203.
(56) Sanders, J. V. *Philos. Mag. A* **1980**, *42*, 705–720.
(57) Murray, M. J.; Sanders, J. V. *Philos. Mag. A* **1980**, *42*, 721–740.
(58) Pusey, P. N.; Vanmegen, W. *Nature* **1986**, *320*, 340–342.
(59) Bartlett, P.; Ottewill, R. H.; Pusey, P. N. *Phys. Rev. Lett.* **1992**, *68*, 3801–3804.
(60) Velikov, K. P.; Christova, C. G.; Dullens, R. P. A.; van Blaaderen, A. *Science* **2002**, *296*, 106–109.
(61) Rupich, S. M.; Shevchenko, E. V.; Bodnarchuk, M. I.; Lee, B.; Talapin, D. V. *J. Am. Chem. Soc.* **2010**, *132*, 289–296.
(62) Zeng, X. B.; Ungar, G.; Liu, Y. S.; Percec, V.; Dulcey, S. E.; Hobbs, J. K. *Nature* **2004**, *428*, 157–160.
(63) Abe, E.; Yan, Y. F.; Pennycook, S. J. *Nat. Mater.* **2004**, *3* 759–767.
(64) Keys, A. S.; Glotzer, S. C. *Phys. Rev. Lett.* **2007**, *99*, 235503.
(65) van Blaaderen, A. *Nature* **2009**, *461*, 892–893.
(66) Evers, W. H.; Friedrich, H.; Filion, L.; Dijkstra, M.; Vanmaekelbergh, D. *Angew. Chem., Int. Ed.* **2009**, *48*, 9655–9657.
(67) Likos, C. N.; Henley, C. L. *Philos. Mag. B* **1993**, *68*, 85–113.
(68) Xu, H.; Baus, M. *J. Phys.: Condens. Matter* **1992**, *4*, L663–L668.
(69) Bishop, K. J. M.; Wilmer, C. E.; Soh, S.; Grzybowski, B. A. *Small* **2009**, *5*, 1600–1630.
(70) Min, Y. J.; Akbulut, M.; Kristiansen, K.; Golan, Y.; Israelachvili, J. *Nat. Mater.* **2008**, *7*, 527–538.
(71) Lalatonne, Y.; Richardi, J.; Pileni, M. P. *Nat. Mater.* **2004**, *3*, 121–125.
(72) Hart, G. L. W. *Nat. Mater.* **2007**, *6*, 941–945.
(73) Leunissen, M. E.; Christova, C. G.; Hynninen, A. P.; Royall, C. P.; Campbell, A. I.; Imhof, A.; Dijkstra, M.; van Roij, R.; van Blaaderen, A. *Nature* **2005**, *437*, 235–240.